Identification of productive and futile encounters in an electron transfer protein complex

Witold Andrałojć[a,b,c], Yoshitaka Hiruma[d], Wei-Min Liu[d], Enrico Ravera[a,b], Masaki Nojiri[e,f], Giacomo Parigi[a,b,c], Claudio Luchinat[a,b,c,1], and Marcellus Ubbink[d,1]

[a]Magnetic Resonance Center (CERM), University of Florence, 50019 Sesto Fiorentino, Italy; [b]Interuniversity Consortium for Magnetic Resonance of Metallo Proteins (CIRMMP), 50019 Sesto Fiorentino, Italy; [c]Department of Chemistry, University of Florence, 50019 Sesto Fiorentino, Italy; [d]Leiden Institute of Chemistry, Leiden University, 2333 CC Leiden, The Netherlands; [e]Department of Chemistry, Graduate School of Science, Osaka University, Osaka 560-0043, Japan; and [f]RIKEN SPring-8 Center, Hyogo 679-5148, Japan

Edited by Harry B. Gray, California Institute of Technology, Pasadena, CA, and approved January 17, 2017 (received for review October 13, 2016)

Well-defined, stereospecific states in protein complexes are often in exchange with an ensemble of more dynamic orientations: the encounter states. The structure of the stereospecific complex between cytochrome P450cam and putidaredoxin was solved recently by X-ray diffraction as well as paramagnetic NMR spectroscopy. Other than the stereospecific complex, the NMR data clearly show the presence of additional states in the complex in solution. In these encounter states, populated for a small percentage of the time, putidaredoxin assumes multiple orientations and samples a large part of the surface of cytochrome P450cam. To characterize the nature of the encounter states, an extensive paramagnetic NMR dataset has been analyzed using the Maximum Occurrence of Regions methodology. The analysis reveals the location and maximal spatial extent of the additional states needed to fully explain the NMR data. Under the assumption of sparsity of the size of the conformational ensemble, several minor states can be located quite precisely. The distribution of these minor states correlates with the electrostatic potential map around cytochrome P450cam. Whereas some minor states are on isolated positively charged patches, others are connected to the stereospecific site via positively charged paths. The existence of electrostatically favorable pathways between the stereospecific interaction site and the different minor states or lack thereof suggests a means to discriminate between productive and futile encounter states.

paramagnetic NMR | encounter complex | cytochrome P450cam | putidaredoxin | maximum occurrence

Crystal structures suggest that proteins assume unique, stereospecific orientations within protein–protein complexes. However, a number of studies in solution have made clear that encounter states are an inherent element of protein complexes (1–8), especially in electron transfer (ET), where the interactions are often extremely fast (9). In the encounter complex, the proteins assume multiple other orientations, often in equilibrium with the major stereospecific state. In low-affinity complexes with dissociation constant (K_d) values > 10 μM, the encounter complex can represent a sizeable fraction, and in some cases, a well-defined, stereospecific complex may even be absent (10–15). The presence of encounter states may be a consequence of the chemical nature of proteins. In nonobligate stereospecific complexes, the interface represents a small fraction of the total protein surface, and therefore, it is reasonable to assume that weak interactions also occur elsewhere. In the case in which protein pairs have evolved to exhibit a high association rate by using electrostatic preorientation, electrostatic patches seem to enhance the presence of encounter states (16, 17). On the one hand, the preorientation reduces the surface area that is visited by the partner, thus enhancing the number of productive encounters, but on the other hand, highly charged patches can bind the oppositely charged protein in many orientations with about equal energy, a situation that has been compared with Velcro binding (18).

Cytochrome P450cam (cytP450cam) from *Pseudomonas putida* is the most comprehensively studied member of the ubiquitous superfamily of cytochromes P450—heme-containing monooxygenases involved in a plethora of chemical reactions, including drug metabolism, oxidation of xenobiotics, and the synthesis of steroids, that receive electrons from ET proteins (19). CytP450cam catalyzes the stereo- and regiospecific hydroxylation of camphor to 5-exo-hydroxycamphor. The reaction involves two one-electron reduction steps, with electrons transferred from NADH via putidaredoxin (Pdx) reductase and Pdx. Studies in vitro have elucidated an intriguing difference between these two ET steps by showing that the first can be achieved by a variety of reducing agents, whereas the second strictly requires the presence of Pdx (20–22). This behavior has raised much interest in the molecular details of the cytP450cam–Pdx interaction over the last three decades. However, the crystal and solution structures of the ET complex formed by the two molecules were solved only very recently by X-ray crystallography and paramagnetic NMR (23, 24). The relative orientation of the proteins within the complex in the solution and crystalline states is practically identical, consistent with the information available from the mutagenesis studies of the system and favorable for effective ET (21, 25–29). It is still under debate whether Pdx induces opening of substrate-bound cytP450cam. The crystal structures showed that, in the complex, cytP450cam was present in the open state, with the F and G helices moved aside to allow substrate access to the active site. However, a recent solution study using paramagnetic NMR provided evidence that, at ambient temperature in solution,

Significance

Paramagnetic NMR spectroscopy is exquisitely sensitive for sparsely populated states in protein–protein interactions, and thus, it can provide important information on how protein–protein complexes form and evolve toward their productive state. However, the description of ensembles of protein–protein orientations is nontrivial, and great care must be taken when deriving biologically relevant results. We have applied an algorithm that restricts the conformational space sampled by the two partners to the maximum allowed for by the data. These ensembles can then be reduced assuming the principle of scarcity. We found that some states are linked to the main state through electrostatic pathways. Such paths help to identify those minor states that are able to evolve into the productive complex.

Author contributions: G.P., C.L., and M.U. designed research; W.A., Y.H., E.R., and M.N. performed research; W.-M.L. contributed new reagents/analytic tools; W.A. and Y.H. analyzed data; and W.A., E.R., G.P., C.L., and M.U. wrote the paper.

The authors declare no conflict of interest.

This article is a PNAS Direct Submission.

Data deposition: The crystallography, atomic coordinates, and structure factors have been deposited in the Protein Data Bank, www.wwpdb.org (PDB ID code 5GXG).

[1]To whom correspondence may be addressed. Email: luchinat@cerm.unifi.it or m.ubbink@chem.leidenuniv.nl.

This article contains supporting information online at www.pnas.org/lookup/suppl/doi:10.1073/pnas.1616813114/-/DCSupplemental.

cytP450cam remains closed on binding to Pdx (30). Low-temperature EPR studies suggested that Pdx binding leads to a mixture of open and closed states for the oxidized cytP450cam but not for the reduced, CO-bound state (31, 32). Modeling work supports a view that Pdx binding does affect the active site, enabling the catalytic reaction and perhaps leading to partial opening of the substrate access channel (33).

The stereospecific complex that was found in solution did not explain all of the paramagnetic NMR data measured for the system, which was already pointed out by Hiruma et al. (24). One of the paramagnetic probes introduced into cytP450cam induces much stronger paramagnetic relaxation enhancements (PREs) for multiple amide protons in Pdx than predicted by the stereospecific structure, suggesting that the latter does not represent a complete picture of the interaction of cytP450cam with Pdx in solution. The PREs unaccounted for by both the solution and crystal structures (called from now on the main state or the stereospecific complex) thus report on the presence of either a minor binding site or an encounter complex. At the same time, most NMR observables—pseudocontact shifts (PCSs), residual dipolar couplings (RDCs), and a significant part of PREs—are very well-reproduced by a single structure. This observation strongly suggests that the population of the additional state(s) is small, but a low population does not necessarily imply the absence of a functional role. The goal of this work was to shed more light on the presence of these minor states by making use of a significantly enlarged paramagnetic NMR dataset obtained by introducing additional paramagnetic probes on the surfaces of the two proteins and recently developed methods to analyze multiple conformational states (34, 35) by exploiting paramagnetism-derived restraints.

When a paramagnetic tag is attached to one of the interacting proteins, the PCSs, RDCs, and PREs measured for the partner protein report on the reciprocal position and orientation of the two macromolecules. If some mobility is present between the two proteins, then the measured PCSs, RDCs, and under specific assumptions, also PREs are simple population-weighted averages of the values that would have been measured for the individual sampled states provided that the states interconvert rapidly on all of the different timescales determined by the PCS, RDC, and PRE (36, 37) (fast exchange regime). We have treated this as a fast exchange system, because binding and dissociation of Pdx and cytP450cam are fast on the chemical shift timescale, and internal mobility within the complex is likely to be much faster. We have also assumed the correlation time for the PREs to be the reorientation correlation time of the whole complex, which represents a safe choice, because it leads to overestimation of the PRE effect that, in turn, reflects into an overestimation of the expected size of the regions discussed in *Results and Discussion*, *Identifying the Minor States by minOR Calculations* (*SI Text*). The exquisite sensitivity of PREs to the presence of even very sparsely populated states—as long as they are located close to the paramagnetic probe—is well-recognized and a direct consequence of the particularly strong distance dependence of the PRE effect ($\sim r^{-6}$). Conformers located very close to the paramagnetic probe, in fact, can account for PREs orders of magnitude higher than when they are located farther away, and thus, even a marginally small population of such states can easily dominate the measured (ensemble-averaged) PREs. A similar behavior does not apply to RDCs (which are independent of the distance between the nuclei and the paramagnetic tag) and is much weaker for the PCSs (which depend on r^{-3}). Therefore, PREs can reveal the existence of very small populations of conformers that may remain hidden when analyzing PCSs and RDCs only.

Although the combined use of PCSs, RDCs, and PREs yields a wealth of highly complementary pieces of information on the reciprocal position and orientation of the two interacting proteins, in the presence of mobility, the problem of recovering a conformational ensemble from averaged data remains highly underdetermined, because an infinite number of different ensembles can reproduce the measured data equally well. This important issue has been widely studied, and a variety of methodologies has been developed by different groups (38–41) to extract information (i.e., plausible conformational ensembles) from such conformationally averaged data (reviewed in ref. 42). One of such methods consists of assigning to each conformer a value, called Maximum Occurrence (MaxOcc), which is defined as the highest fraction of time for which this conformer can exist in any optimized conformational ensemble without causing violations of the experimental averaged data (34, 37, 43–47). It, thus, provides an upper bound for the population of each conformer in the real conformational ensemble of the system.

The concept of MaxOcc was subsequently generalized from single structures to groups of conformers (or regions in the conformational space), giving rise to Maximum Occurrence of Regions (MaxOR) and minimum Occurrence of Regions (minOR) analysis (35). The minOR calculations permit us to identify conformational regions that must necessarily be sampled by the system to reproduce the experimental data. In fact, the minOR is the smallest population that the considered region must have in any conformational ensemble capable of reproducing the averaged data. In this work, the motionally averaged PREs are analyzed in conjunction with PCSs, RDCs, and the available protein structures to extract the information that they contain on the sampling of minor states in the complex between cytP450cam and Pdx. So far, the MaxOR/minOR methods have been applied to characterize relative motions between protein domains linked by flexible parts of the polypeptide chain and a helix–bulge–helix RNA element (48). In the current study, this approach is used to characterize encounter states. In an encounter state, the proteins can, in theory, assume any relative orientation, making the number of possibilities much larger than in the case of domain motions. The strategy is based on the identification of the conformational regions, distinct from the stereospecific complex, that must be sampled to fulfill the data (i.e., with minOR > 0). Our analysis shows that over 10 such regions exist, in several cases spread over parts of the conformational space that are very distant from the main interaction site. We also show that, if sparsity assumptions about the nature of the conformational sampling are made, the minor states become much better defined, and plausible models for the internal motion in the complex can be proposed. The locations of the identified minor states correlate with the surface charge distributions of the two proteins, suggesting that they represent an electrostatically driven encounter complex that may have mechanistic implications.

Results and Discussion

Assessing the Contribution of the Stereospecific Interaction Site. The dataset used in this study is greatly enlarged with respect to the original paper (24). The double-armed caged lanthanoid NMR probe #7 (CLaNP-7) (49) was introduced in two new positions, 272/276 (probe 2) and 195/199 (probe 5), on the surface of cytP450cam (Fig. 1), yielding two additional sets of PREs and one additional set of PCSs and RDCs (because no intermolecular PCSs were observed for probe 5). Another set of PREs was also recorded by labeling the Pdx with a (1-oxyl-2,2,5,5-tetramethyl-3-pyrroline-3-methyl)-methanesulfonothioate (MTSL) spin label on C73 (probe 6). The data recorded previously consisted of PCSs, RDCs, and PREs obtained by placing the CLaNP-7 probe in positions 126/130 (probe 1) and 333/337 (probe 3) of cytP450cam as well as position 6/12 of Pdx (probe 4). A summary of the experimental restraints is given in Table S1.

A recent crystal structure [Protein Data Bank (PDB) entry 5GXG] of the protein complex was refined against both X-ray and NMR data (see SI Text and Table S2) and used for subsequent analysis. A global analysis of the NMR data was performed to determine the compatibility with the previously identified main state (PDB entry 2M56) (24). The goal is threefold: (*i*) to check whether it remains the most favored conformer when the new data

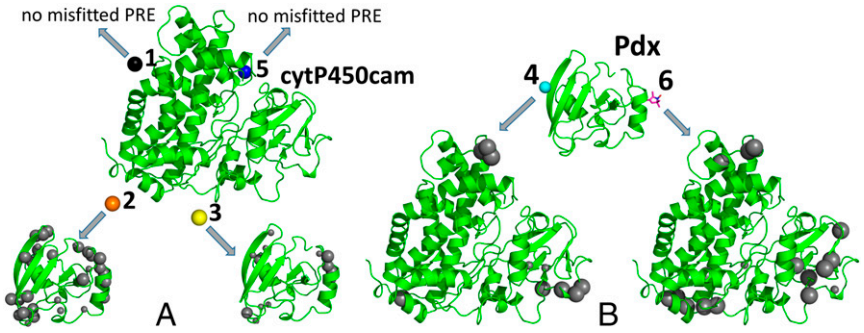

Fig. 1. Paramagnetic lanthanoid/MTSL tag positions and distribution of PREs unaccounted for by the main state of the complex. For each paramagnetic probe, the amide protons of the reporter protein with PREs unaccounted for by the main state are indicated by gray spheres—large spheres signify strongly misfitted PREs (used to construct the clusters), and smaller spheres signify moderately (~20 s^{-1}) misfitted ones. (*A*) Probes placed on cytP450cam (PREs measured on Pdx). (*B*) Probes placed on Pdx (PREs measured on cytP450cam).

are included in the analysis, (*ii*) to identify the experimental PREs that cannot be accounted for by the main state (even allowing for some local mobility), and (*iii*) to determine the upper and lower limits of its population. The compatibility of all available restraints with the proposed main state for the complex was monitored by calculating the MaxOcc of each structure in a densely sampled, broad pool of sterically allowed conformations of the complex, possibly relevant for the fit of the experimental data (*Materials and Methods* and *SI Text*). The largest MaxOcc value calculated for a single conformer is 99.4%, and the corresponding structure has the center of mass of Pdx translated by only 1.3 Å and rotated by 6° with respect to the position of the best scoring conformer of the previously published NMR family (PDB ID code 2M56) as calculated by superimposing the cytP450cam structures. This conformation is practically within the breadth of the NMR family itself. This result shows that the additional paramagnetic NMR data confirm the structure of the stereospecific complex (PDB ID code 2M56) determined previously as the "main state." It also indicates that this state can represent the structure of the complex with a weight up to more than 99% without causing any violations of the experimental data. At the same time, however, several tens of PREs are strongly misfitted—some of them by more than 100 s^{-1}—if the weight of the main state is increased to 100% (Q_{PRE} = 0.69) as depicted in Figs. 1 and 2. These large violations, thus, leave no doubt that additional conformations are sampled by the system. It should be recalled that the real weight of the main state can be actually smaller than 99.4%, because MaxOcc represents the upper limit for the occurrence of a conformation (see below).

To check whether the PREs in disagreement with the main state can be explained by a limited local mobility, the MaxOR of a conformational region comprising all of the conformers with Pdx within 5-Å translation and 10° rotation from the main state was calculated. The MaxOR of this region is 99.5%, and it reproduces the PREs only marginally better (Q_{PRE} = 0.60) than the single conformer with the largest MaxOcc, showing that local mobility cannot be the main cause of the unexpectedly high PREs. More than 50 PREs (caused by four different paramagnetic probes) are actually significantly underestimated (by more than 30 s^{-1} or if the PRE itself is smaller than that, 20 s^{-1}). To obtain a first crude estimate of how broad the conformational sampling should be, the MaxOR calculations were performed by gradually increasing the size of the region built around the main state. It was found (Table S3) that the smallest region with MaxOR of 100.0% that can yield a good fit of all data must contain conformers with Pdx translated up to 55 Å and rotated up to 100° from the main state (i.e., must span a significant fraction of the whole conformational space available to the complex). This finding does not imply that this whole region must be populated but shows that the system must sample conformers located far from the main state.

Identifying the Minor States by minOR Calculations. A PRE that cannot be accounted for by the main state (Figs. 1 and 2) reports the proximity of a nucleus and a paramagnetic center in a conformation that exists for a fraction of time. The PRE is essentially isotropic and thus, depends only on the metal–nuclear distance, and therefore, the PRE leaves a large degeneracy in the position of the nucleus relative to the center. If conformational regions are generated by translation and rotation of Pdx (in the fixed frame of cytP450cam) with respect to the main state, as was done above, these regions will comprise a large number of structures not fulfilling the distance constraint to include all conformations that do. The presence of so many structures makes it unclear which conformations are really important to fit the data. Therefore, more informative conformational regions were introduced. Below, we describe the steps to filter out the conformers most relevant to describe the experimental data, with the underlying assumptions made at each step.

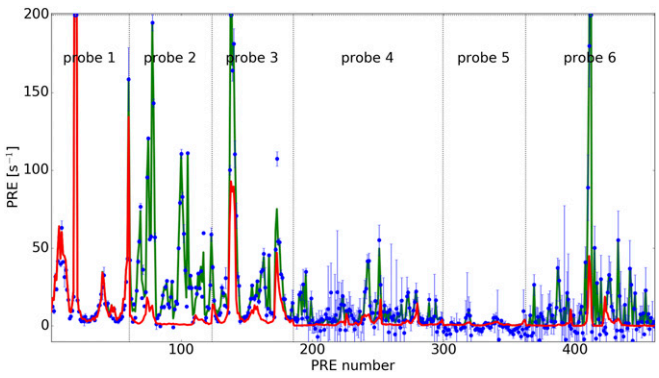

Fig. 2. Observed and calculated PREs. The experimental PREs are shown as blue dots, the PREs back-calculated from the main state alone are shown as a red line, and those from an ensemble containing 99.4% of the main state complemented with 0.6% of other conformers optimized to fit the experimental data are shown as a green line. The complementing structures were selected from the broad conformational pool (in the text), and their specific weights were chosen through the ensemble optimization algorithm of the MaxOR/minOR program. The error bars represent propagated errors based on the noise level in the NMR spectra and the fitted error in the determination of the diamagnetic transverse relaxation rate. The errors for probes 4 and 6 are noticeably higher because of the lower intensity of the cytP450cam-detected spectra.

A minimal spherical region around a given probe was defined that still contains conformers that cannot all be left out to explain the restraints produced by that probe (minOR > 0). Given the relation between the probe–nucleus distance in a conformer and the population of that conformer (weight), in principle, that region becomes very large if the population of the conformer goes up, because a larger population allows for conformers at a larger distance to experience a given PRE. However, in defining these regions, all restraints were evaluated. The PCSs, RDCs, and PREs from other probes restrict the weight that a region as a whole can attain, thus limiting the size of the region. Furthermore, only Pdx molecules located close to the cytP450cam surface were considered to represent physically possible complexes (*SI Text*). Given the large population of the main state, each encounter region is expected to have quite a low population, and for this reason, all regions with minOR > 0 were selected.

To define a limited number of regions, we assumed that PREs of structurally close nuclei induced by the same paramagnetic probe are likely probing the same minor state(s) and that those PREs were clustered for the definition of the regions (details on the clustering procedure are in *SI Text*, and Fig. S1 depicts the positions on the protein structures of the nuclei of which the PREs were clustered). In this way, 12 clusters were defined containing between one and nine observations each. The clusters were labeled using letter codes (A–L) preceded by the number of the probe that caused the specific PREs.

The sizes of the smallest regions with minOR > 0 as well as their MaxOR are listed in Table S4. The table also reports the size that each region would need to have to include the main interaction site. This value indicates how distant each cluster is from the main state. These distances confirm that none of the defined regions contain the main interaction site (as expected), although some of them have their borders very close to it. Examples of regions are shown in Fig. 3 *A*, region 2.C and *D*, region 6.L, and all of the identified regions are depicted in Fig. S2. Many regions exhibit some overlap, and in some cases, the structures in the overlap areas can fit the PREs of both regions simultaneously, suggesting that, in principle, all of these PREs could report on the same minor state (the discussion in *SI Text* has details). Table S5 identifies these overlapping regions. This observation is important for the discussion of the number of the detected minor states.

The three regions constructed from the PREs induced by probe 2 on Pdx nuclei share no conformations that explain all PREs simultaneously (Table S5). This lack of overlap means that at least three clearly distinct orientations of Pdx located next to this probe have to be sampled in the Pdx–cytP450cam encounter complex. These three regions (2.A, 2.B, and 2.C), although spanning a similar range of positions of Pdx with respect to cytP450cam (Fig. S2 *A*–*C*), are, in fact, defined by Pdx conformers with different orientations. This conclusion is illustrated in Fig. 3*B*, in which the frame of reference is that of Pdx. For probe 3, also on cytP450cam, region 3.E overlaps with both regions 3.D and 3.F, which in turn, are mutually exclusive, meaning that at least two different groups of structures close to that probe have to be sampled. However, several overlaps exist between regions related to probes 2 and 3, so that the three states required by probe 2 could also simultaneously fit all data related to probe 3. Thus, three distinct minor states are sufficient to fit all of the data originating from probes 2 and 3. Of course, it cannot be concluded that only three states must exist; it only shows that, if one makes the explicit assumption of looking for a solution with the smallest number of states, three would be enough.

Analogously, for the other two probes (probes 4 and 6 located on the Pdx), no overlaps are present between the six different regions related to the corresponding PREs. As far as the regions induced by the same probe are concerned, this conclusion may have been expected, because owing to the large size of cytP450cam, the clusters of nuclei defining the different regions are well-separated from one another (Fig. 1). The lack of overlap between the regions of probes 4 and 6 indicates that the two probes report on distinct orientations of Pdx.

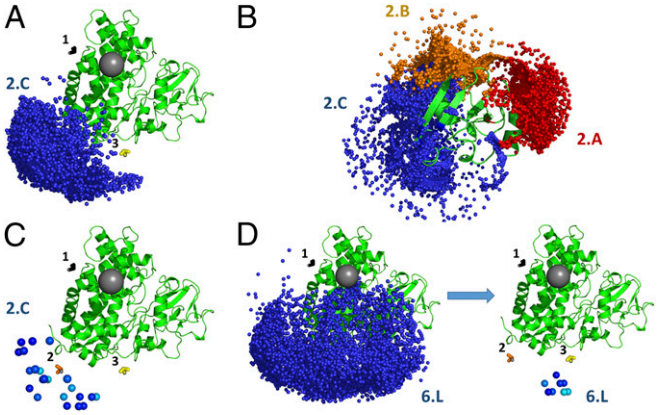

Fig. 3. Representative minOR regions and their counterparts shrunk by assuming sparsity. (*A*) The smallest region with minOR > 0 for cluster 2.C; cytP450cam is shown as a green cartoon, with the positions of probes 1–3 indicated as black, orange, and yellow axis frames, respectively; the blue dots represent the centers of mass of Pdx in all of the conformations belonging to the region, and the gray sphere indicates the position of Pdx in the stereospecific complex. (*B*) The three regions with minOR > 0 for probe 2 [clusters A (red), B (orange), and C (blue)] represented in the Pdx frame of reference; Pdx is shown in green cartoon, and the blue dots mark the positions of probe 2 (on cytP450cam) in all of the conformations composing the regions. (*C*) The subsections of the region shown in *A* (cluster 2.C) obtained by applying an assumption of sparsity (in the text): each sphere marks the center of a 5 × 5 × 5-Å cube, and the different shades of blue denote the quality of the fit [from dark blue ($Q = 0$) to light blue ($Q = 0.2$)]. (*D*) Region 6.L before (*Left*) and after (*Right*) applying the assumption of sparsity (represented as in *A* and *C*, respectively).

The presence of overlaps between regions related to probes 2 and 3 (labeled A–F) on one side and probes 4 and 6 (G–L) on the other side suggests that some of the data related to probes 4 and 6 can actually be explained by conformations present in the regions defined from probes 2 and 3. In particular, region 4.I overlaps with most of the regions of probes 2 and 3, which is not surprising, because the cytP450cam residue central in defining this region for probe 4 (I275) is located very close to the attachment site of probe 2 on the surface of cytP450cam (C272/C276).

Finding the Most Representative Minor States by Applying an Assumption of Sparsity. The regions considered in the previous section contain all of the structures that can possibly be used to account for specific subsets of PREs. Their borders, sizes, and relations (overlaps) constitute the safe information that can be obtained from the available PREs without making any assumption on the characteristics of the conformational ensemble of the complex other than the rigidity of the proteins. The cost of this generality is that most regions are very broad and do not offer a detailed description of the system in terms of sampled conformational states.

We are now going to consider whether making some reasonable assumptions about the characteristics of the real conformational ensemble can significantly restrict the number of possible solutions and provide more precise information on the ensemble itself. We apply the Occam's razor principle [an assumption with precedents in NMR conformational analyses (50); i.e., we aim to describe the experimental data with a minimum set of solutions]. Reaching this goal could involve exploiting the overlaps between the regions, which is discussed in the previous section. Moreover, the assumption of sparsity allows one to limit the size of the regions themselves.

Small sets of conformers needed to fit all of the PREs related to a given cluster were determined by splitting the regions into cubes of 5 × 5 × 5 Å and then, fitting the experimental data using the main

state complemented by the conformers present in one of the cubes. If the fit of the PREs related to the probe in this cluster is almost as good as that obtained when the whole region is taken (as calculated from the Q factor), then the cube represents a possible sampled state; otherwise, it is discarded. Analogous to the determination of the regions discussed above, the combined weight of the conformers within the cube was limited by fitting all restraints for all nuclei and including the main state. Because fitting the PCSs and RDCs requires a large weight for the main state, this approach is an efficient way to limit the weight of any conformer in an encounter state.

With this approach, several regions (mostly those for probes 4 and 6) were shrunk considerably and in four cases, practically reduced to well-defined states (regions 4.G, 4.I, 6.J, and 6.L) (Fig. 3 and Fig. S2). Each cube in these 12 shrunk regions has minOR = 0, but still, when any of the cubes, one for each region, are taken together and complemented with the main state, they are in good agreement with the experimental data.

A Model for Futile and Productive Encounter States. At this point, it is possible to analyze the relation between the various regions in functional terms. It is clear that the encounter complex in the Pdx–cytP450cam complex represents a small fraction but covers a large surface area. Encounter states close to the main state are thought to enhance the association rate by reducing the diffusional search dimensions (51). The farther an encounter conformer is from the main state, the larger the chance that the complex will dissociate before the partners have reached the main state and the association is complete. Such states are called futile encounter complexes (52, 53). If they represent a significant fraction, they reduce the association rate, because they effectively represent a competitive binding site that is inactive. Thus, we wondered whether the encounter complexes described here are isolated or connected to the main state, which could provide evidence that Pdx can easily diffuse to (and from) the main state. In the latter case, the minor states could represent productive rather than futile encounter states and enhance the association rate. The possible connections were hypothesized by inspecting whether electrostatically favorable pathways for the exchange with the main state exist as well as whether the PRE data indicate the presence of intermediate states along such pathways. The Pdx surface is mostly negatively charged as is a significant part of the cytP450cam surface. The most prominent positively charged zone of the cytP450cam surface is located at the main binding site for Pdx.

We first consider the four minor states that are already relatively well-defined. Most of them are located far from the main state, and if they were to represent productive encounter states, several connecting intermediate states should exist and be detected by PRE measurements. Of these well-defined minor states, one (region 6.L) lays on the surface of cytP450cam opposite to the main state (Fig. 4). Interestingly, this minor state is positioned directly over a small positively charged patch on cytP450cam. This patch extends toward the attachment site of probe 3 and reaches the main interaction site. The entire pathway is located in the zone of conformational space, where the structures necessary to fit the PREs sensed by probe 3 are located (yellow mesh in Fig. 4). Based on this electrostatic path to the main state and the likely presence of conformers on this path, it can be hypothesized that region L of probe 6 represents a productive encounter location. Two other well-defined minor states (regions 4.G and 6.J) are located very close to each other (but Pdx has clearly distinct orientations), and their exact positions can be selected, such that they are placed over positively charged zones of cytP450cam. In this case, however, the positive patch does not extend toward the main state, and also, no obvious intermediate conformations can be selected from the minor-derived regions, suggesting that the observed interactions at this site are futile. The last well-defined state (region 4.I) is located on the same side of cytP450cam as the main state but close to the attachment site of probe 2. The surface potential map suggests that it can either directly exchange with the main state or do so through intermediates that can be selected from the regions defined using probe 2 (orange mesh in Fig. 4). Finally, two other regions (regions 4.H and 6.K) contain conformers that are very close to the main state and thus, can directly exchange with it. The positive patch around the main interaction site is actually somewhat broader than the interface of the stereospecific complex, and interestingly, it extends exactly toward the part of space in which regions 4.H and 6.K are located and in the opposite direction toward probe 2 and region 4.I, while ending right after the main interaction site in the direction of probe 1 (for which no additional PREs were observed). To complete the discussion of correlations between the positions of the minor states and the electrostatic potential map of cytP450cam, it is worth noting that no minor states were identified in the whole zone of helices F and G (covering the substrate entry channel), which is strongly negatively charged. This finding is not caused by lack of paramagnetic probe coverage in this area,

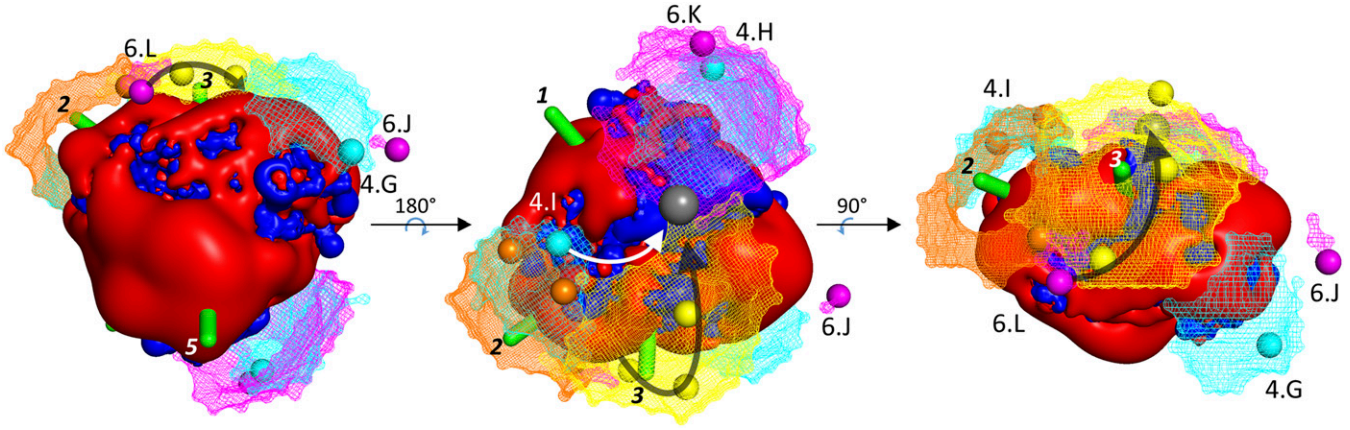

Fig. 4. The positive (blue) and negative (red) electrostatic potential isosurfaces [obtained using APBS (61) and traced in PyMol (62) at 0.7 kT/e] of cytP450cam are depicted together with the center of mass positions of Pdx in the encounter regions obtained after applying the scarcity assumption (see text) shown as a mesh, with the colors representing the states related to the different probes; probe 2, orange; probe 3, yellow; probe 4, cyan; probe 6, magenta. The colored spheres are representatives of the respective encounter regions placed above positively charged surface areas. The gray sphere represents the main state. The green bars indicate the probe positions on cytP450cam. The curved arrows indicate possible paths between the minor states and the main binding site, suggesting that these states could represent productive encounter sites. Regions 4.G and 6.J illustrate isolated states that may represent futile encounter sites.

because probe 5 is attached to helix G, and therefore, it shows that no relevant interactions are occurring in this area.

The surface of cytP450cam features one other zone of positive potential covering a part of its surface exactly opposite to the main interaction site, but none of the identified regions are located next to it. Actually, almost no PREs were sensed by the residues in that zone (the highest PRE being 11 s^{-1}), suggesting that, also in this part of the protein, no interaction occurs. In general, however, the PRE-derived regions and the surface charge distribution of cytP450cam coincide surprisingly well.

Conclusions

The very good sensitivity of PREs to minor states coupled to the application of the MaxOcc methodology to tackle the analysis of motionally averaged data allowed us to identify a series of lowly populated states that together populated a small percentage at maximum in the presence of a strongly dominating major conformation of cytP450cam in complex with Pdx. The MaxOR/minOR method alone traces the outer borders of the possible spatial extent of these states as reported by the available PRE data. Because of the large indetermination of the ensemble recovery problem as well as the intrinsic insensitivity of PREs to certain type of motions, this result represents all of the information that the available experimental data can provide without assumptions on the type of conformational heterogeneity of the system.

We expect this method of identifying the possible conformers in the encounter state to be generally applicable to any protein–protein complex characterized by transient interactions. However, it is important that the free proteins, all conformers of the encounter state and the stereospecific state, are in fast exchange compared with the timescale defined by the PREs. In the cases of very large PREs observed for nuclei of conformers close to the paramagnetic probe, this condition may not always be met, leading to an underestimation of the large PREs. Therefore, it is recommended to use a lower boundary for large PREs. The introduction of probes can affect the formation of the stereospecific complex. Such an effect can be detected easily by changes in chemical shift perturbations or reduced affinity, and such probe positions should be discarded. However, the effect of probes on the encounter state is harder to establish. Thus, the description of the encounter state should be based on multiple probes to reduce the disturbing effect that individual probes may have. Last, it is important that the initial pool of structures used for the MaxOR/minOR method samples the possible orientations of the two proteins as extensively as possible.

Under a single regularizing assumption, the MaxOR/minOR results permit us to propose a plausible model for the interaction between Pdx and cytP450cam. The minor states determined within this model point toward an electrostatic nature of the underlying interaction, because the center of mass of the mostly negative Pdx seems to follow the positive patches present on the surface of cytP450cam. With the approach described here, it has been possible to formulate hypotheses about which families of conformers represent productive encounters and which ones are futile. These hypotheses can be tested by modification of the surface using site-directed mutagenesis or with computational approaches.

Materials and Methods

Chemicals. CLaNP-7 was synthesized and loaded with Lu^{3+}, Gd^{3+}, and Tm^{3+} ions as described (49); MTSL and (1-acetyl-2,2,5,5-tetramethyl-3-pyrroline-3-methyl)-methanesulfonothioate (MTS) were purchased from Toronto Research Chemicals.

Mutagenesis. To prepare double-cysteine mutants of Pdx and cytP450cam, site-directed mutagenesis was carried out using QuikChange protocol (Stratagene).

Protein Production. Pdx and cytP450cam variants were produced as previously described (24).

Paramagnetic Probe Attachments. Pdx and cytP450cam variants were labeled with Ln^{3+}-CLaNP-7 as previously described (24). For MTS/MTSL tagging, Pdx WT was incubated with 5 mM DTT in 20 mM potassium phosphate, pH 7.0, and 50 mM KCl for 30 min on ice. DTT was removed by using a PD-10 column. The protein solution was mixed with five molar equivalents of MTS/MTSL and incubated for 1 h at 4 °C. Oligomers and surplus of spin labels were removed by two steps of chromatography. The MTS/MTSL-incubated sample was filtered and loaded on a HiTrap Q HP anion-exchange column (2 mL). The protein was eluted with a linear gradient of 0.1–0.4 M KCl in 20 mM potassium phosphate, pH 7.4, and the first peak fractions were collected and subsequently loaded on a Superose 12 size exclusion column preequilibrated with 50 mM Tris·HCl, pH 7.4, 100 mM KCl, 1 mM camphor, 1% (vol/vol) MeOH, and 6% (vol/vol) D_2O. The eluted brown fractions were pooled and concentrated. Approximately 80–90% of protein was lost during the labeling procedure, presumably because MTSL labeling reduces the stability of the iron sulfur cluster.

NMR Samples and Experiments. NMR samples contained 100–200 μM [^{2}H, ^{15}N] Pdx (WT) or [^{2}H, ^{15}N] cytP450cam (C334A) with two molar equivalents Ln^{3+}-CLaNP-7–labeled cytP450cam or Ln^{3+}-CLaNP-7/MTS/MTSL–tagged Pdx mutants, respectively, in 50 mM Tris·HCl, pH 7.4, 100 mM KCl, 1 mM camphor, and 7% (vol/vol) D_2O; 2D ^{15}N-^{1}H HSQC and ^{15}N-^{1}H TROSY spectra (54) were recorded at 290 K on a Bruker Avance III 600-MHz spectrometer equipped with a TCI-Z-GRAD cryoprobe.

NMR Assignment. All NMR data were processed in NmrPipe (55) and analyzed in CCPNMR (56). The amide resonances of oxidized Pdx and cytP450cam were assigned based on previous works (24, 57).

Data Analysis. PCS and RDC measurements were performed as previously described (24). PRE datasets of Gd^{3+}-CLaNP-7 and MTSL were analyzed as reported before (10, 24). Briefly, the peak heights of the amide resonances of the proteins in the presence of partner protein with either a diamagnetic probe (Lu^{3+}-CLaNP-7 or MTS) or a paramagnetic probe (Gd^{3+}-CLaNP-7 or MTSL) were represented as I_{dia} and I_{para}, respectively. The I_{para}/I_{dia} ratios were normalized by dividing them by the averaged values of the 10 largest I_{para}/I_{dia} values (0.96, 1.15, 1.09, 0.95, 1.0, and 0.97 for cytP450cam probe positions 1, 2, 3, and 5; Pdx probe position 4; and MTSL, respectively). The PREs values ($R_{2,para}$) were calculated as described (58). All experimental PCS, RDC, and PRE values are listed in Tables S6–S8.

MaxOcc and MaxOR/minOR Calculations. The MaxOR of a given group of conformers is calculated by finding ensembles optimized to simultaneously (*i*) fit the experimental data within a certain threshold and (*ii*) include the highest population of the conformers in question. The appropriate ensembles can be found by solving the linear optimization problem defined by

$$\underset{\mathbf{x}}{\operatorname{argmin}} \left\{ \|\mathbf{A}\mathbf{x}-\mathbf{y}\|_2^2 - \gamma \sum_{i \in C} x_i + \lambda \left(1 - \sum_{i=1}^{N} x_i\right)^2 \right\} \text{ s.t. } \mathbf{x} \geq 0, \qquad [1]$$

where $\mathbf{x}$ is the vector of the weights of the N structures composing the considered pool of conformers; $\mathbf{y}$ is the vector of M experimentally observed values of PCSs, RDCs, and PREs normalized by their respective norms; and $\mathbf{A}$ is the $M \times N$ matrix with columns that contain the PCS, RDC, and PRE values back-calculated for each of the conformers (*SI Text*), again normalized by the norm of the experimental data. Note that this normalization of the $\mathbf{y}$ vector and the $\mathbf{A}$ matrix makes the term $\|\mathbf{A}\mathbf{x}-\mathbf{y}\|_2^2$ correspond to the sum of squares of the Q factors (59) between the experimental and back-calculated data for PCSs, RDCs, and PREs. This term reflects the fit of the experimental data. The maximization of the population of the considered region is achieved by the second term, in which C denotes the set of the structures within the considered region. The third term constrains the sum of populations of all of the structures to one.

The second term is a regularization, and as such, it has an adverse effect on the quality of reproduction of the experimental data (it will tend to increase the weight of a certain group of conformers not necessarily well-suited to fit the experimental data); thus, the weighting factor γ is introduced to control the influence of this term.

During a MaxOR calculation, γ is first set to zero, and **1** is solved to obtain the best possible fit of the available experimental data (lowest sum of Q factors or $\|\mathbf{A}\mathbf{x}-\mathbf{y}\|_2^2$). Every ensemble that can fit the experimental data within a threshold set 30% higher than the minimum value obtained from **1** in the best possible fit is considered to reproduce the experimental data in a satisfactory matter.

After the best achievable value of $\|\mathbf{Ax}-\mathbf{y}\|_2^2$ is established, the calculations are repeated for increasing γ-values. By increasing γ, the population of the considered region increases, and at the same time, the agreement with the experimental data decreases. The value of γ at which the quality of the fit matches the 30% threshold is found through a 1D bisection method. The total population of the considered region ($\sum_{i\in C} x_i$) found for this value of γ is, thus, the highest that can exist without causing a misfit of the experimental data—and as such, it is the MaxOR of this region.

The other weighting factor λ depends on the specific experimental dataset, and its value is found with the L-curve method as a compromise between a good fit of the experimental observables and the proximity of the sum of the weights to one (in a minimization in which term 2 is not present) (60). A value of 10 was used in these calculations.

The calculation of minOR proceeds in the same way, with the only difference being that the second term is now taken with a positive sign. In this way, the population of the considered region is forced to be as small as possible.

Also, for calculating the MaxOcc of a given single conformation, **1** is used, with the set *C* containing only the single conformer under examination.

ACKNOWLEDGMENTS. Discussions with Prof. Charalampos Kalodimos and Prof. Gottfried Otting are acknowledged. This research was supported by the People Programme (Marie Curie Actions) of European Union's Seventh Framework Programme FP7/2007-2013/ under Research Executive Agency Grant 317127 (pNMR), Fondazione Cassa di Risparmio di Firenze, Ministero dell'Istruzione, dell'Università e della Ricerca (MIUR) Progetti di Ricerca di Interesse Nazionale (PRIN) Grant 2012SK7ASN, European Commission Project Bio-MedBridges 284209, and Instruct, part of the European Union European Strategy Forum on Research Infrastructures, through its Core Centre "Magnetic Resonance Center," Florence, Italy. E.R. holds a Fondazione Italiana Ricerca sul Cancro (FIRC) Triennial Fellowship Gino Mazzega and Guglielmina Locatello (17941). W.-M.L., Y.H. and M.U. were supported by VICI Grant 700.58.441 (to M.U.) from The Netherlands Organization for Scientific Research (NWO). The X-ray diffraction studies were performed at beamline 44XU in the synchrotron radiation facility SPring-8 (Proposals 2013A6841 and 2013B6841) and supported by the Japan Society for the Promotion of Science (JSPS) KAKENHI Grant 23750190 and grants from Japan Foundation for Applied Enzymology and Takeda Science Foundation.

1. Anthis NJ, Clore GM (2015) Visualizing transient dark states by NMR spectroscopy. *Q Rev Biophys* 48(1):35–116.
2. Bashir Q, Scanu S, Ubbink M (2011) Dynamics in electron transfer protein complexes. *FEBS J* 278(9):1391–1400.
3. Van de Water K, van Nuland NAJ, Volkov AN (2014) Transient protein encounters characterized by paramagnetic NMR. *Chem Sci* 5(11):4227–4236.
4. Schilder J, Ubbink M (2013) Formation of transient protein complexes. *Curr Opin Struct Biol* 23(6):911–918.
5. Ubbink M (2012) Dynamics in transient complexes of redox proteins. *Biochem Soc Trans* 40(2):415–418.
6. Clore GM, Iwahara J (2009) Theory, practice, and applications of paramagnetic relaxation enhancement for the characterization of transient low-population states of biological macromolecules and their complexes. *Chem Rev* 109(9):4108–4139.
7. Clore GM (2008) Visualizing lowly-populated regions of the free energy landscape of macromolecular complexes by paramagnetic relaxation enhancement. *Mol Biosyst* 4(11):1058–1069.
8. Schreiber G, Keating AE (2011) Protein binding specificity versus promiscuity. *Curr Opin Struct Biol* 21(1):50–61.
9. Gray HB, Winkler JR (1996) Electron transfer in proteins. *Annu Rev Biochem* 65(1): 537–561.
10. Scanu S, et al. (2012) The complex of cytochrome f and plastocyanin from Nostoc sp. PCC 7119 is highly dynamic. *ChemBioChem* 13(9):1312–1318.
11. Scanu S, Foerster JM, Ullmann GM, Ubbink M (2013) Role of hydrophobic interactions in the encounter complex formation of the plastocyanin and cytochrome f complex revealed by paramagnetic NMR spectroscopy. *J Am Chem Soc* 135(20):7681–7692.
12. Scanu S, Foerster JM, Timmer M, Ullmann GM, Ubbink M (2013) Loss of electrostatic interactions causes increase of dynamics within the plastocyanin-cytochrome f complex. *Biochemistry* 52(38):6615–6626.
13. Xu X, et al. (2008) Dynamics in a pure encounter complex of two proteins studied by solution scattering and paramagnetic NMR spectroscopy. *J Am Chem Soc* 130(20): 6395–6403.
14. Liang ZX, et al. (2002) Dynamic docking and electron transfer between Zn-myoglobin and cytochrome b(5). *J Am Chem Soc* 124(24):6849–6859.
15. Worrall JAR, et al. (2002) Myoglobin and cytochrome b5: A nuclear magnetic resonance study of a highly dynamic protein complex. *Biochemistry* 41(39):11721–11730.
16. Schreiber G, Haran G, Zhou H-X (2009) Fundamental aspects of protein-protein association kinetics. *Chem Rev* 109(3):839–860.
17. Ubbink M (2009) The courtship of proteins: Understanding the encounter complex. *FEBS Lett* 583(7):1060–1066.
18. McLendon G (1991) Control of biological electron transport via molecular recognition and binding: The "velcro" model. *Long-Range Electron Transfer in Biology (Structure and Bonding)*, ed Palmer G (Springer, Berlin), pp 159–174.
19. Ahuja S, et al. (2013) A model of the membrane-bound cytochrome b5-cytochrome P450 complex from NMR and mutagenesis data. *J Biol Chem* 288(30):22080–22095.
20. Lipscomb JD, Sligar SG, Namtvedt MJ, Gunsalus IC (1976) Autooxidation and hydroxylation reactions of oxygenated cytochrome P-450cam. *J Biol Chem* 251(4):1116–1124.
21. Tosha T, Yoshioka S, Ishimori K, Morishima I (2004) L358P mutation on cytochrome P450cam simulates structural changes upon putidaredoxin binding: The structural changes trigger electron transfer to oxy-P450cam from electron donors. *J Biol Chem* 279(41):42836–42843.
22. Pochapsky SS, Pochapsky TC, Wei JW (2003) A model for effector activity in a highly specific biological electron transfer complex: The cytochrome P450(cam)-putidaredoxin couple. *Biochemistry* 42(19):5649–5656.
23. Tripathi S, Li H, Poulos TL (2013) Structural basis for effector control and redox partner recognition in cytochrome P450. *Science* 340(6137):1227–1230.
24. Hiruma Y, et al. (2013) The structure of the cytochrome p450cam-putidaredoxin complex determined by paramagnetic NMR spectroscopy and crystallography. *J Mol Biol* 425(22):4353–4365.
25. Holden M, Mayhew M, Bunk D, Roitberg A, Vilker V (1997) Probing the interactions of putidaredoxin with redox partners in camphor P450 5-monooxygenase by mutagenesis of surface residues. *J Biol Chem* 272(35):21720–21725.
26. Unno M, Shimada H, Toba Y, Makino R, Ishimura Y (1996) Role of Arg112 of cytochrome p450cam in the electron transfer from reduced putidaredoxin. Analyses with site-directed mutants. *J Biol Chem* 271(30):17869–17874.
27. Hiruma Y, et al. (2014) Hot-spot residues in the cytochrome P450cam-putidaredoxin binding interface. *ChemBioChem* 15(1):80–86.
28. Koga H, et al. (1993) Essential role of the Arg112 residue of cytochrome P450cam for electron transfer from reduced putidaredoxin. *FEBS Lett* 331(1-2):109–113.
29. Yoshioka S, Takahashi S, Ishimori K, Morishima I (2000) Roles of the axial push effect in cytochrome P450cam studied with the site-directed mutagenesis at the heme proximal site. *J Inorg Biochem* 81(3):141–151.
30. Skinner SP, et al. (2015) Delicate conformational balance of the redox enzyme cytochrome P450cam. *Proc Natl Acad Sci USA* 112(29):9022–9027.
31. Myers WK, Lee Y-T, Britt RD, Goodin DB (2013) The conformation of P450cam in complex with putidaredoxin is dependent on oxidation state. *J Am Chem Soc* 135(32): 11732–11735.
32. Liou S-H, Mahomed M, Lee Y-T, Goodin DB (2016) Effector roles of putidaredoxin on cytochrome P450cam conformational states. *J Am Chem Soc* 138(32):10163–10172.
33. Hollingsworth SA, Batabyal D, Nguyen BD, Poulos TL (2016) Conformational selectivity in cytochrome P450 redox partner interactions. *Proc Natl Acad Sci USA* 113(31): 8723–8728.
34. Bertini I, et al. (2010) Conformational space of flexible biological macromolecules from average data. *J Am Chem Soc* 132(38):13553–13558.
35. Andrałojć W, Luchinat C, Parigi G, Ravera E (2014) Exploring regions of conformational space occupied by two-domain proteins. *J Phys Chem B* 118(36):10576–10587.
36. Iwahara J, Schwieters CD, Clore GM (2004) Ensemble approach for NMR structure refinement against (1)H paramagnetic relaxation enhancement data arising from a flexible paramagnetic group attached to a macromolecule. *J Am Chem Soc* 126(18): 5879–5896.
37. Bertini I, Luchinat C, Nagulapalli M, Parigi G, Ravera E (2012) Paramagnetic relaxation enhancement for the characterization of the conformational heterogeneity in two-domain proteins. *Phys Chem Phys* 14(25):9149–9156.
38. Berlin K, et al. (2013) Recovering a representative conformational ensemble from underdetermined macromolecular structural data. *J Am Chem Soc* 135(44):16595–16609.
39. Salmon L, Bascom G, Andricioaei I, Al-Hashimi HM (2013) A general method for constructing atomic-resolution RNA ensembles using NMR residual dipolar couplings: The basis for interhelical motions revealed. *J Am Chem Soc* 135(14):5457–5466.
40. Camilloni C, Vendruscolo M (2015) Using pseudocontact shifts and residual dipolar couplings as exact NMR restraints for the determination of protein structural ensembles. *Biochemistry* 54(51):7470–7476.
41. Chen J-L, et al. (2016) 3D structure determination of an unstable transient enzyme intermediate by paramagnetic NMR spectroscopy. *Angew Chem Int Ed Engl* 55(44): 13744–13748.
42. Ravera E, Sgheri L, Parigi G, Luchinat C (2016) A critical assessment of methods to recover information from averaged data. *Phys Chem Phys* 18(8):5686–5701.
43. Bertini I, et al. (2007) Paramagnetism-based NMR restraints provide maximum allowed probabilities for the different conformations of partially independent protein domains. *J Am Chem Soc* 129(42):12786–12794.
44. Longinetti M, Luchinat C, Parigi G, Sgheri L (2006) Efficient determination of the most favoured orientations of protein domains from paramagnetic NMR data. *Inverse Probl* 22(4):1485–1502.
45. Bertini I, et al. (2012) MaxOcc: A web portal for maximum occurrence analysis. *J Biomol NMR* 53(4):271–280.
46. Luchinat C, Nagulapalli M, Parigi G, Sgheri L (2012) Maximum occurrence analysis of protein conformations for different distributions of paramagnetic metal ions within flexible two-domain proteins. *J Magn Reson* 215(1):85–93.
47. Dasgupta S, et al. (2011) Narrowing the conformational space sampled by two-domain proteins with paramagnetic probes in both domains. *J Biomol NMR* 51(3):253–263.
48. Andrałojć W, et al. (2016) Inter-helical conformational preferences of HIV-1 TAR-RNA from maximum occurrence analysis of NMR data and molecular dynamics simulations. *Phys Chem Chem Phys* 18(8):5743–5752.
49. Liu W-M, et al. (2012) A pH-sensitive, colorful, lanthanide-chelating paramagnetic NMR probe. *J Am Chem Soc* 134(41):17306–17313.

50. Clore GM, Schwieters CD (2004) How much backbone motion in ubiquitin is required to account for dipolar coupling data measured in multiple alignment media as assessed by independent cross-validation? *J Am Chem Soc* 126(9):2923–2938.
51. Delbrück M, Adam G (1968) Reduction of dimensionality in biological diffusion processes. *Structural Chemistry and Molecular Biology*, eds Rich A, Davidson N (Freeman, San Francisco), pp 198–215.
52. Harel M, Spaar A, Schreiber G (2009) Fruitful and futile encounters along the association reaction between proteins. *Biophys J* 96(10):4237–4248.
53. Fawzi NL, Doucleff M, Suh JY, Clore GM (2010) Mechanistic details of a protein-protein association pathway revealed by paramagnetic relaxation enhancement titration measurements. *Proc Natl Acad Sci USA* 107(4):1379–1384.
54. Pervushin K, Riek R, Wider G, Wüthrich K (1997) Attenuated T2 relaxation by mutual cancellation of dipole-dipole coupling and chemical shift anisotropy indicates an avenue to NMR structures of very large biological macromolecules in solution. *Proc Natl Acad Sci USA* 94(23):12366–12371.
55. Delaglio F, et al. (1995) NMRPipe: A multidimensional spectral processing system based on UNIX pipes. *J Biomol NMR* 6(3):277–293.
56. Vranken WF, et al. (2005) The CCPN data model for NMR spectroscopy: Development of a software pipeline. *Proteins* 59(4):687–696.
57. Lyons TA, Ratnaswamy G, Pochapsky TC (1996) Redox-dependent dynamics of putidaredoxin characterized by amide proton exchange. *Protein Sci* 5(4):627–639.
58. Battiste JL, Wagner G (2000) Utilization of site-directed spin labeling and high-resolution heteronuclear nuclear magnetic resonance for global fold determination of large proteins with limited nuclear overhauser effect data. *Biochemistry* 39(18): 5355–5365.
59. Cornilescu G, Marquardt JL, Ottiger M, Bax A (1998) Validation of protein structure from anisotropic carbonyl chemical shifts in a dilute liquid crystalline phase. *J Am Chem Soc* 120(27):6836–6837.
60. Andrałojć W, et al. (2015) Information content of long-range NMR data for the characterization of conformational heterogeneity. *J Biomol NMR* 62(3): 353–371.
61. Baker NA, Sept D, Joseph S, Holst MJ, McCammon JA (2001) Electrostatics of nanosystems: Application to microtubules and the ribosome. *Proc Natl Acad Sci USA* 98(18): 10037–10041.
62. Schrödinger LLC (2015) The PyMOL Molecular Graphics System, Version 1.8 (Schrödinger, LLC, New York).
63. Rinaldelli M, et al. (2014) Simultaneous use of solution NMR and X-ray data in REFMAC5 for joint refinement/detection of structural differences. *Acta Crystallogr D Biol Crystallogr* 70(Pt 4):958–967.
64. García de la Torre J, Huertas ML, Carrasco B (2000) HYDRONMR: Prediction of NMR relaxation of globular proteins from atomic-level structures and hydrodynamic calculations. *J Magn Reson* 147(1):138–146.
65. Clarkson RB, et al. (1998) Multi-frequency EPR determination of zero field splitting of high spin species in liquids: Gd(III) chelates in water. *Mol Phys* 95(6):1325–1332.
66. Hudson A, Lewis JWE (1970) Electron spin relaxation of ^{8}S ions in solution. *Trans Faraday Soc* 66:1297–1301.